

Optimized textural features for mass classification in digital mammography using a weighted average gravitational search algorithm

Oludare Yinka Ogundepo¹, Isaac Ozovehe Avazi Omeiza², Jonathan Ponnile Oguntayo³

¹Department of Electrical and Electronics Engineering, College of Technology, Federal University of Petroleum Resources, Effurun, Nigeria

²Department of Electrical and Electronics Engineering, Faculty of Engineering and Technology, University of Ilorin, Ilorin, Nigeria

³Department of Computer Engineering, Faculty of Engineering and Technology, Ladoko Akintola University of Technology, Ogbomoso, Nigeria

Article Info

Article history:

Received Apr 18, 2021

Revised Feb 3, 2022

Accepted Apr 6, 2022

Keywords:

Breast cancer

Digital mammography

Gabor filter

Gravitational search algorithm

Gray level co-occurrence matrices

Support vector machine

Texture features

ABSTRACT

Early detection of breast cancer cells can be predicted through a precise feature extraction technique that can produce efficient features. The application of Gabor filters, gray level co-occurrence matrices (GLCM) and other textural feature extraction techniques have proven to achieve promising results but were often characterized by a high false-positive rate (FPR) and false-negative rate (FNR) with high computational complexities. This study optimized textural features for mass classification in digital mammography using the weighted average gravitational search algorithm (WA-GSA). The Gabor and GLCM features were fused and optimized using WA-GSA to overcome the weakness of the textural feature techniques. With support vector machine (SVM) used as the classifier, the proposed algorithm was compared with commonly applied techniques. Experimental results show that the SVM with WA-GSA features achieved FPR, FNR and accuracy of 1.60%, 9.68% and 95.71% at 271.83 s, respectively. Meanwhile, SVM with Gabor features achieved FPR, FNR and accuracy of 3.21%, 12.90% and 93.57% at 2351.29 s, respectively, while SVM with GLCM features achieved FPR, FNR and accuracy of 4.28%, 18.28% and 91.07% at 384.54 s, respectively. The obtained results show the prevalence of the proposed algorithm, WA-GSA, in the classification of breast cancer tumor detection.

This is an open access article under the [CC BY-SA](https://creativecommons.org/licenses/by-sa/4.0/) license.



Corresponding Author:

Oludare Yinka Ogundepo

Department of Electrical and Electronics Engineering, College of Technology, Federal University of Petroleum Resources

Effurun, Delta State, Nigeria

Email: oludare.ogundepo@fupre.edu.ng

1. INTRODUCTION

Digital mammography is a powerful technique that helps in the diagnosis of breast cancers at premature stages [1]. The early detection of breast cancer helps prevent the growth to a complicated stage which could lead to the need for surgeries. This forestalls unnecessary biopsies and radiation therapies by proper screening and abnormality detection; thus, increases the likelihood of patient's survival [2], [3]. The malignancy can be found in patients in the presence of masses and microcalcifications in the breast region. The successful analysis of breast cancer relies on features extracted from the cancer suspicious areas and classification of the features using a classifier or the combinations of classifiers [4], [5]. The enrichment and

extraction of regions of interest (ROI) in digital images is the foremost challenging task in the computerized diagnosis of breast cancer using mammographic images. This is due to low contrast results which are sometimes complicated to handle two major concerns namely false-positives and false-negatives [6]. The false-positive results could lead to the surgeries of benign (noncancerous) conditions. Meanwhile, the false-negative results could allow the early-stage disease to develop to a more complicated stage with fewer rates of survival.

Computer-aided detection and diagnosis (CAD) can be utilized on the digital images to assist radiologists analyze the overall images, and emphasize the likely areas of concern for further analysis [7]. The two significant phases of a CAD system for mass detection are the detection of suspicious ROI in mammogram images and the classification of these ROI into the masses (malignant) or normal cases. One of the critical stages in the classification of ROI is feature extraction, which absolutely affects the classification rate [2]. An assortment of computer-aided methods has recently been examined and it produced different levels of success for the analysis of the digital mammograms [8].

Gravitational search algorithm (GSA) is an efficient optimization algorithm created based on mass interactions and the law of gravity [9]. The GSA uses the Newtonian gravity's theory, and its explorer agents are the set of masses. In GSA, there is a system of masses such that every mass in the system is matched with the location of other masses using the gravitational force. This force is a way of passing information between different masses [10].

Gabor filter is a method which has been largely used for a textural description in different imaging applications [3]. Gabor filters decompose an image into different scales and orientations and analyze texture patterns efficiently. Mammograms have high texture, and Gabor filters are suitable for the texture analysis of mammograms as well [11].

The gray level co-occurrence matrices (GLCM) is a second-order statistical method that calculates the frequency of pixel pairs having the same grey-levels in an image and applies additional knowledge obtained using spatial pixel relations [12]–[15]. GLCM has been largely used for image texture analysis [16]. It was applied as a feature extraction technique to compute the textural measure. The co-occurrence matrix reveals the grey level spatial dependency along with different angular relationships, horizontal, vertical and two diagonal directions on an image. The co-occurrence matrix embeds the distribution of grayscale transitions using edge information. Since most of the information required for computing threshold values are embedded in GLCM, it has emerged as a basic yet efficient technique [17].

Khan *et al.* [18] proposed improved Gabor features for mass classification in mammography. The study introduced optimization of Gabor filter banks based on an increasing clustering algorithm and particle swarm optimization (PSO). SVM with Gaussian kernel as a fitness function for PSO was utilized and assessed on 1024 ROI extracted from a digital database for screening mammography (DDSM) using four performance measures (i.e., accuracy, area under receiver operating characteristic (ROC) curve, sensitivity, and specificity). The outcomes showed that the proposed technique improves performance and diminishes the computational cost. Shirazi and Rashedi [10] projected a feature weighting for cancer tumor detection in mammography images using a GSA with GLCM as the feature extraction technique. The GSA was used as a tool for the optimization of the features weighting (FW) and tuning the classifier (k-NN). The weighted features and the tuned k-NN classifier were utilized for discovering tumors. The obtained results showed a good efficiency of GSA-based FW-kNN classification for breast cancer tumor detection. Hussain *et al.* [19] presented a comparison of different Gabor features for mass classification in mammography. The study explored the performance of six different Gabor feature extraction approaches for mass classification problems. The technique employed Gabor filter banks for extracting multiscale and multi-orientation texture features which represent structural characteristics of masses and normal dense tissues in mammograms. The feature extraction approaches were evaluated over the ROI extracted from MIA'S database. The support vector machine (SVM) was used to effectively classify the generated unbalanced datasets. The experimental outcome revealed that the proposed method was able to reduce the false positives and false negatives. However, it is computationally expensive and time-consuming.

Reliable CAD systems are developed for robust feature extraction techniques for mass detection. To improve the efficiency and accuracy of a CAD system, it is crucial to extract the most discriminative features efficiently [2]. All the aforementioned textural feature extraction techniques developed for efficient mass detection in early breast cancer CAD diagnosis are quite robust. However, they are restricted by high tendency rate of false positive and false negative diagnosis. Also, there are mostly associated with high computational complexities. To address these limitations, this study aims to develop a hybrid technique for textural feature extraction in breast cancer diagnosis. The specific objectives are: i) to fuse the Gabor and GLCM textural feature extraction technique using the weighted average gravitational search algorithm (WA-GSA) technique, ii) to apply the developed hybrid technique to some selected mammographic images for training and testing, and iii) to compare the performance of the new hybrid technique with the existing

ones based on accuracy, false-positive rate, false-negative rate, and computational time. Next, section 2 showcases the detailed research method while the results are given in section 3. Section 4 concludes the study and contains the recommendation for further studies.

2. RESEARCH METHOD

Digital mammographic images including normal, benign, and cancerous cases were first acquired. Then, the images were pre-processed to obtain the desired image quality for further processing. This is followed by obtaining the ROI boundaries, edges and curves of the pre-processed images and the result are subsequently segmented. Gabor filter texture segmentation and extraction is performed before classification. The features of the obtained dataset are extracted based on the developed algorithm before being classified for training and testing.

2.1. Image acquisition

Digital mammographic images were acquired from the image retrieval in medical applications (IRMA) database of the Aachen University of Technology Germany. This dataset provides 9,852 radiographs, which include normal, benign, and cancerous cases. Each study includes two images of each breast, acquired in craniocaudal (CC) and medio-lateral (ML) views that have been scanned from the film-based sources by four different scanners with a resolution between 50 and 42. For this study, seven hundred (700) digital mammographic images were selected. Four hundred and twenty (420) of the acquired images were used for training while two hundred and eighty (280) of the images were used for the testing. The test dataset comprises 93 normal mammogram images and 187 abnormal mammogram images: out of which 92 were benign mammogram images and 95 cancerous mammogram images.

2.2. Pre-processing

A series of pre-processing steps were applied to improve the image quality for further processing. The acquired images were passed unto different pre-processing techniques and image resizing was performed. Thereafter, the removal of the black and white border, breast boundary detection, artefacts elimination (labels) and background, removal of the pectoral muscle and contrast adjustment. The pre-processing techniques were Otsu's method for thresholding, Moore's Algorithm for tracing boundary on threshold images, and difference of Gaussians (DOG) as contrast enhancement technique. The outputs at different stages of the pre-processing stages using DOG is depicts in Figure 1, where Figure 1(a) is the original image, Figure 1(b) is black and white removal, Figure 1(c) is the flipped image, Figure 1(d) is the traced boundary, Figure 1(e) is the pectoral muscle removal, Figure 1(f) is the enhanced image CLAHE, Figure 1(g) is the enhanced image DOG, Figure 1(h) is the Gaussian blur image, Figure 1(i) ROI_image, Figure 1(j) is the Shannon entropy image, and Figure 1(k) is the morphological filtering image. The methodologies associated with the stages are discussed elsewhere [20].

2.3. Segmentation

The ROI boundaries, edges and curves of the pre-processed images were located and segmented using Gaussian blurring, Otsu's thresholding, and automatic cropping technique. Fuzzy C-means clustering was applied to the ROI and the evaluations of the textual image were done using a GLCM. Shannon's Entropy-based thresholding was performed on the GLCM texture and morphological filtering were finally applied. The output produced the excepted segmented image. Gabor filter was also used for the segmentation process in the case of the Gabor filter feature extraction. The steps involved in fuzzy C-means image segmentation are highlighted elsewhere [21] and are:

- Initialize the cluster centers c_i and set $t = 0$.
- Initialize the fuzzy partition memberships functions μ_{ij} according to (1).

$$\mu_{ij} = \left(\sum_{m=1}^C \left(\frac{\|x_j - c_i\|}{(\|x_j - c_m\|)^{2/(k-1)}} \right) \right)^{-1} \quad (1)$$

- Let $t = t + 1$ and compute new cluster centres c_i using (2).

$$c_i = \frac{\sum_{j=1}^N \mu_{ij}^k x_j}{\sum_{j=1}^N \mu_{ij}^k} \quad (2)$$

- Repeat steps 2 to 3 until convergence.

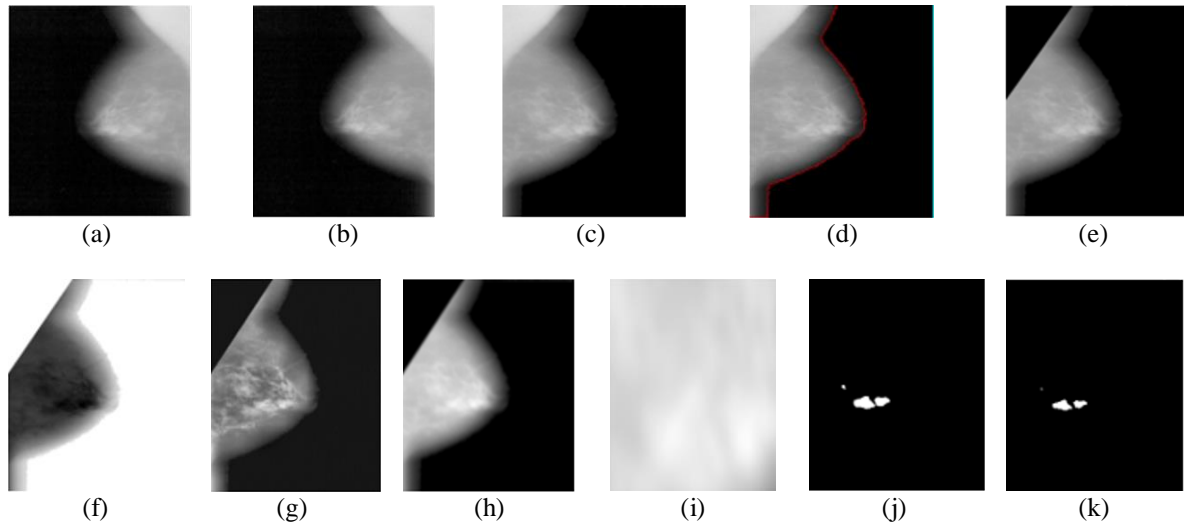


Figure 1. Summary of the pre-processing stage (a) original image, (b) black and white removal, (c) flipped image, (d) traced boundary, (e) pectoral muscle removal, (f) enhanced image CLAHE, (g) enhanced image DOG, (h) Gaussian blur image, (i) ROI_image, (j) Shannon entropy image, and (k) morphological filtering image

2.4. Gabor filter texture segmentation and extraction

The texture is considered to be the most important property for masses representation since it is useful for characterizing micro patterns like edges, lines, and spots. Gabor filter has been used with different scales and orientations to extract texture-based features [19], [22]. The filters have been applied in the various domains of computer science such as face recognition, gesture recognition, and optical character recognition. Gabor is highly efficient in the CAD system as mammogram contains micropattern which has a lot of texture [3]. A 2-D Gabor filter defined as a Gaussian function modulated by an oriented complex sinusoidal wave can be described as given in (3) [23]:

$$g(x, y) = \frac{1}{2\pi\sigma_x\sigma_y} e^{[-1/2((x^2/\rho_x^2)+(\bar{y}^2/\sigma_y^2))]} e^{(2\pi jw\bar{x})} \tag{3}$$

where \bar{x} and \bar{y} are expressed as given in (4) and (5)

$$\bar{x} = x\cos\theta + y\sin\theta \tag{4}$$

$$\bar{y} = x\sin\theta + y\cos\theta \tag{5}$$

σ_x and σ_y are the scaling parameters (i.e., they define the neighbourhood of a pixel where the weighted summation takes place), W is the central frequency of the complex sinusoid and $\theta \in [0, \pi]$ is the orientation of the normal to the parallel stripes of the Gabor function.

Gabor filter was used to segment the mammogram dataset before feature extraction was carried out. The segmentation of the images using the Gabor filter is portrayed in Figure 2. The input image $i(x, y)$ was expected to be composed of two textures.

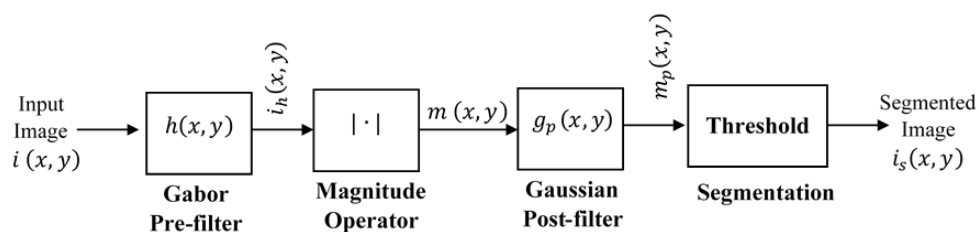


Figure 2. Segmentation using Gabor filter

The image was first passed through a Gabor pre-filter with impulse response $h(x, y)$. The Gabor function $h(x, y)$ (see (6)) is a complex sinusoid centred at a frequency (U, V) and modulated by a Gaussian envelope $g(x, y)$ (in (7)). The spatial extent of the Gaussian envelope is determined by the parameter σ_g .

$$h(x, y) = g(x, y) \exp[-j2\pi(Ux + Vy)] \quad (6)$$

and

$$g(x, y) = \frac{1}{2\pi\sigma_g^2} \exp\left[-\frac{(x^2+y^2)}{2\pi\sigma_g^2}\right] \quad (7)$$

Further, the 2D Fourier transform of $h(x, y)$ is

$$H(u, v) = G(u - U, v - V) \quad (8)$$

where

$$G(u, v) = \exp[-2\pi^2\sigma_g^2(u^2 + v^2)] \quad (9)$$

is the Fourier transform of $g(x, y)$. The parameters (U, V, σ_g) determine $h(x, y)$. From (7) and (8), the Gabor function is basically a bandpass filter centered around frequency (U, V), with bandwidth determined by σ_g . It was assumed for simplicity, that the Gaussian envelope $g(x, y)$ is an asymmetrical function. The output of the pre-filter stage $i_h(x, y)$ is the convolution of the input image with the filter response

$$i_h(x, y) = h(x, y) * i(x, y) \quad (10)$$

The magnitude of the first-stage output is computed in the second stage as expressed in (11):

$$m(x, y) = |i_h(x, y)| = |h(x, y) * i(x, y)| \quad (11)$$

A low-pass Gaussian post-filter $g_p(x, y)$ is applied to pre-filter output $m(x, y)$ yielding the post-filtered image

$$m_p(x, y) = m(x, y) * g_p(x, y) \quad (12)$$

where

$$g_p(x, y) = \frac{1}{2\pi\sigma_p^2} \exp\left[-\frac{(x^2+y^2)}{2\pi\sigma_p^2}\right] \quad (13)$$

Generally, $i_h(x, y)$ is referred to as the pre-filtered image, $m(x, y)$ as the pre-filtered output, and $m_p(x, y)$, the post-filtered output. Finally, the segmented image $i_s(x, y)$ from the Gaussian-post-filter output $m_p(x, y)$ was achieved by applying a threshold τ to $m_p(x, y)$; points above the threshold are assigned to one texture, and points below to the other.

The segmented image was extracted. The Gabor filter-based technique was used to extract the textural features of the mammography images. Gabor filters are orientation and frequency selective filters, relying upon different parameters, specifically, a frequency f and an orientation θ . Forty different Gabor filters (5 frequency x 8 orientation) were used in this study. The segmented ROI were each partitioned into sub-windows then Gabor filter bank was applied on each window separately. The moments were computed (mean, standard deviation, skewness) based features from the magnitude of Gabor filter bank responses to obtain a one thousand and eighty (1080) texture feature set.

2.5. GLCM algorithm for feature extraction

In this study, fourteen textural features namely angular second moment (energy), correlation, contrast, entropy, homogeneity, inverse difference moment, the sum of entropy, sum variance, the sum of average, different average, difference variance, different entropy, information measures correlation 1 and information measures correlation 2 were employed. The GLCM was computed for the four directions around the pixel of interest. The method used an 8x8 sliding window to allow the co-occurrence calculation and extraction of the textural features. The fourteen textural features for the co-occurrence matrices considered

four directions (0° , 45° , 90° and 135°) and distance of one ($d=1$). The fourteen texture features were computed from the GLCM to obtain 56 textures feature set (4 directions x 1 distance x 14 texture features) for each sliding window.

2.6. Normalization of features

The textural features of the mammography images extracted by the respective GLCM and Gabor were normalized using the min-max technique by the aid of (14) and (15):

$$f_{glcm} = \frac{f'_{glcm} - \min(f'_{glcm})}{\max(f'_{glcm}) - \min(f'_{glcm})} \quad (14)$$

$$f_{gabor} = \frac{f'_{gabor} - \min(f'_{gabor})}{\max(f'_{gabor}) - \min(f'_{gabor})} \quad (15)$$

where f'_{glcm} and f'_{gabor} are the features obtained using GLCM and Gabor respectively, while f_{glcm} and f_{gabor} are the normalized features.

2.7. Optimal feature selection

The general formulation of an optimal feature selection problem used in this study are:

$$\min_{K_{best}, F_f^d} \emptyset(y(F_f^d)) \quad (16)$$

Subject to:

$$0 \leq h(x(t), z(t), w(t), K_{best}, F^d) \leq 1 \quad (17)$$

$$F^d \in F_e$$

$$0 < w(t) < 1$$

$$w(t) = \begin{cases} m_j(t) & \text{if } m_j(t) \geq w(t) \\ w(t) & \text{otherwise } m_j(t) < w(t) \end{cases} \quad (18)$$

where $x(t) \in R^n$ and $z(t) \in R^n$ are the vectors of the GLCM and Gabor state variables, respectively. The entire state vector is denoted as $y = [x \ z]$, where x is the set of feature vector of GLCM, z is the set of feature vector of Gabor filter bands. The problem is defined on the feature's horizon $F_e = [F_o^d \ F_f^d]$.

The feature-dependent control variables $K_{best} \in R^n$ and possibly the final feature F_f^d are decision variables for optimization. The goal of the optimization is to find the optimal set of decision variables to minimize the objective function \emptyset , that is, $\emptyset(y(F_f^d))$. The search space for finding the optimum is restricted by constraints, which describe, appropriate weight and feature parameter requirements to be fulfilled during fusion at feature selection level. The study considered weight constraint $w(t)$ and feature constraint $h(\dots)$.

2.8. Weighted average gravitational search algorithm

WA-GSA was used to fuse the normalized features. This was achieved by modifying the fitness function of the GSA using (19):

$$fit_j(t) = \sum_{j=1}^N w(t) f_{glcm_j}(t) + (1 - w(t)) f_{gabor_j}(t) \quad (19)$$

where $\omega(t)$ is the weight of the GLCM features and $(1 - \omega(t))$ is the weight of the Gabor features.

Feature level fusion can be done either at the feature extraction stage or at the feature selection stage. The weighted average method has been used previously as fusion technique and was able to suppress noises existing in the source feature images. At the same time, it also suppresses the salient features that should be preserved for the fused feature image, thereby, producing a low contrast result. In order to reduce the challenge of the weighted average and to have a balanced feature fusion, WA-GSA was developed and employed in this study.

WA-GSA fusion technique was used at the feature selection phase which dealt with the selection and combination of GLCM and Gabor features to remove redundant and irrelevant features, the objective is

to reduce the computational burden of feature concatenation by choosing optimal subsets of features from the two textural features. WA-GSA technique used the following parameters for fusing GLCM features and Gabor features: a maximum iteration of 100, number of agents (N) as the maximum size of the feature vector. The algorithmic steps for the WA-GSA technique used to achieve the fusion are highlighted:

- Step 1: Set f_{gabor} =Gabor features and f_{glcm} =GLCM features
- Step 2: Agents initialization: The positions of the N number of agents are initialized randomly.

$$X_i = (x_i^1, \dots, x_i^d, \dots, x_i^n) \text{ for } i = 1, 2, \dots, N \quad (20)$$

$$w(t) = rand \quad 0 < w(t) < 1$$

x_i^d represents the positions of the i^{th} agent in the d^{th} dimension, while n is the space dimension. $w(t)$ represent the initial weight.

- Step 3: Fitness evolution and best fitness computation. The fitness evolution is performed by evaluating the best and worst fitness for all agents at each iteration. For minimization problems, the best and worst fitnesses are expressed as given in (21):

$$fit_j(t) = \sum_{j=1}^N w(t)f_{glcm_j}(t) + (1 - w(t))f_{gabor_j}(t) \quad (21)$$

Subject to

$$w(t) = \begin{cases} m_j(t) & \text{if } m_j(t) \geq w(t) \\ w(t) & \text{otherwise } m_j(t) < w(t) \end{cases} \quad (22)$$

where $w(t)$ is the weight set for f_{gabor} (Gabor features extracted from mammography image) and $1 - w(t)$ is the weight set for f_{glcm} (GlcM features extracted from mammography image).

$$best(t) = \min fit_j(t) \quad worst(t) = \max fit_j(t) \text{ for } j \in 1, \dots, N$$

For maximization problems best and worst fitness are:

$$best(t) = \max fit_j(t) \quad j \in 1, \dots, N \quad worst(t) = \min fit_j(t) \quad j \in 1, \dots, N$$

$fit_j(t)$ represents the fitness value of the i^{th} agent at iteration t , $best(t)$ and $worst(t)$ represents the best and worst fitness at iteration t .

- Step 4: Gravitational constant (G) computation. The gravitational constant $G(t)$ is computed using (23).

$$G(t) = G_0 e^{(-\alpha t/T)} \quad (h) \quad (23)$$

G_0 and α are initialized at the beginning and was reduced with time to control the search accuracy. T is the total number of iterations.

- Step 5: Calculation of the masses of the agents. Gravitational and inertia masses for each agent are calculated at iteration t . Masses in GSA depend upon the fitness value of agents.

$$M_{aj} = M_{pi} = M_{ii} = M_i \quad i = 1, 2, \dots, N$$

$$m_i(t) = \frac{fit_i - worst(t)}{best(t) - worst(t)} \quad M_i = \frac{m_i(t)}{\sum_{j=1}^N m_j(t)} \quad (24)$$

Where M_{ii} and M_{pi} are inertia and passive gravitational masses of i^{th} agent respectively and M_{aj} is the active gravitational mass of j^{th} agent. fit_i is the fitness value of i^{th} agent.

- Step 6: Calculation of the agent's accelerations: The acceleration of the agents are calculated using (25).

$$a_i^d(t) = \frac{F_i^d(t)}{M_{ii}(t)} \quad (25)$$

$F_i^d(t)$ is the total force acting on i^{th} agent calculated as shown in (26),

$$F_i^d(t) = \sum_{j \in Kbest, j \neq i} rand_j F_{ij}^d(t) \quad (26)$$

$Kbest$ is the set of first K agents with the best fitness value and biggest mass. $Kbest$ will reduce in each iteration and at the end only one agent applying force to the other agents. Force on i^{th} agent by d^{th} agent mass during iteration t is computed using the (27).

$$F_{ij}^d(t) = G(t) \cdot \left(\frac{M_{pi}(t) \times M_{aj}(t)}{R_{ij}(t)} + \varepsilon \right) \cdot (x_j^d(t) - x_i^d(t)) \quad (27)$$

$R_{ij}(t)$ is the Euclidian distance between two agents i and j at iteration t . $G(t)$ is the gravitational constant calculated using (9) while ε is a small constant.

– Step 7: Velocity and positions of agents: The velocity update equation for the agents is defined as given in (28).

$$v_i^d(t+1) = rand_i \times v_i^d(t) + a_i^d(t) \quad (28)$$

$rand$ is random variable in interval $[0,1]$. $v_i^d(t)$ and $v_i^d(t+1)$ are the velocity of i^{th} individual during the iteration t and $t+1$, respectively. The position update equation for individuals is defined as (29).

$$x_i^d(t+1) = x_i^d(t) + v_i^d(t+1) \quad (29)$$

$x_i^d(t)$ and $x_i^d(t+1)$ are the position of i^{th} individual during the iteration t and $t+1$, respectively. The velocity of individuals is updated during each iteration. Due to changes in velocity, every individual updates his position.

– Step 8: Repeat steps 2 to 8. Steps 2 to 8 are repeated until the iterations reach their maximum limit. The best fitness value at the final iteration is computed as the global fitness while the position of the corresponding agent at specified dimensions is computed as the global solution of that particular problem which resulted in the feature selected, $F_{ij}^d(t)$.

$$f_{fused}(t) = F_{ij}^d(t) \quad (30)$$

Where $f_{fused}(t)$ is the fused features at feature selection level.

2.9. Support vector machine for classification

For the classification of features extracted by Gabor and GLCM techniques, SVM was used. In this study, a binary classification problem, where textural features can be characterized as either cancer region or normal was considered. The SVM finds an optimal hyper-plane that can separate the data belonging to different classes with large margins in high dimensional space [24]. The margin is defined as the sum of distances to the decision boundary (hyper-plane) from the nearest points (support vectors) of the two classes. SVM formulation is based on statistical learning theory and has attractive generalization capabilities in linear as well as non-linear decision problems. SVM takes classification decisions using (31) for optimal hyperplane with maximum margin:

$$g(x) = w^T x + w_0 = 0 \quad (31)$$

where x is the feature descriptor and w and w_0 are unknown parameters, which are computed using training samples $\{(x_i, y_i) | 1 \leq i \leq N\}$ where $y_i \in \{+1, -1\}$ is the class label; the computation involves the solution of an optimization problem based on large margin theory [25]. Once the optimal hyper-plane has been computed, the classification of a test sample x is performed using (32):

$$g(x) = \sum_{i=1}^{N_s} \lambda_i y_i x_i^T x + w_0 \quad (32)$$

where λ_i are Lagrange multipliers and N_s is the number of support vectors i.e., the training samples corresponding to non-zero λ_i . In case the data samples belonging to two classes are not linearly separable, the Kernel trick is used. Using a kernel function, the function $g(x)$ is expressed in (33):

$$g(x) = \sum_{i=1}^{N_s} \lambda_i y_i K(x_i, x) + w_0 \quad (33)$$

where $K(x_i, x)$ is the kernel function that expresses the inner product of data. The samples in the higher dimensional space user-defined parameter C is used to control the misclassified penalty or error in the new formulation. The misclassification penalty or error is controlled with a user-defined parameter C (regularization parameter, controlling the trade-off between the error of SVM and margin maximization), and is tied with the kernel. There are several kernels available to be used e.g., linear, polynomial, sigmoid, and radial basis function (RBF) [18]. In this study, the RBF kernel was used as given in (33) and C is set to 2000.

$$K(x_i, x) = \exp(-\gamma \|x_i - x\|^2), \gamma > 0 \tag{34}$$

The γ is the width of the kernel function. RBF kernel is now tied with two parameters γ and C . In summary, Figure 3 summarizes the schematic of the methodology and the process flow.

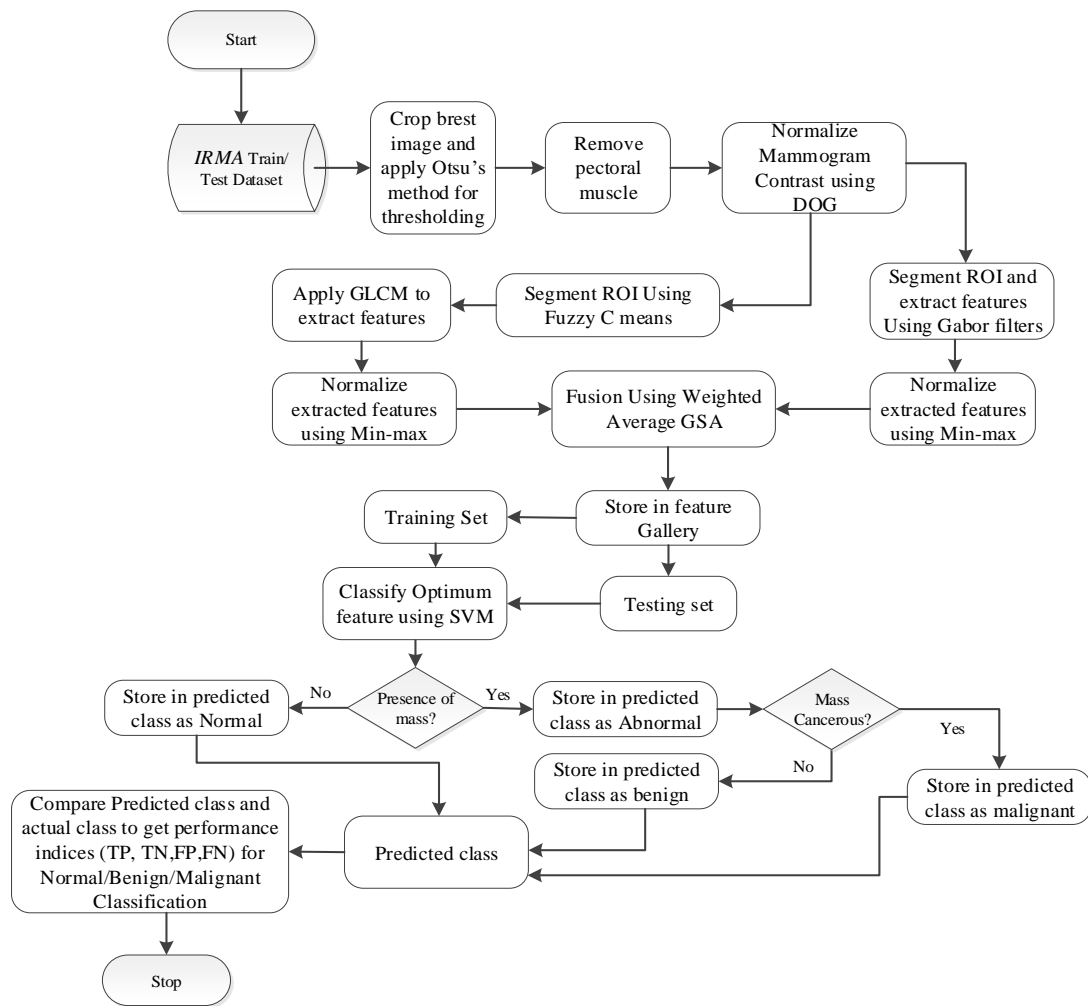


Figure 3. Proposed flow for fused optimization

2.10. Performance evaluation

The overall performance of the techniques under study was evaluated based on recognition accuracy, false positive rate (FPR), false negative rate (FNR) and computation time. A confusion matrix was used to determine the values of the performance metrics. It contains “true positive (TP), false positive (FP), false negative (FN) and true negative (TN)” as expressed in (35)-(37), respectively.

$$\text{False positive rate (FPR)} = \frac{FP}{TN+FP} \tag{35}$$

$$\text{False negative rate (FNR)} = \frac{FN}{TP+FN} \tag{36}$$

$$\text{Accuracy} = \frac{\text{TP}+\text{TN}}{\text{TP}+\text{TN}+\text{FP}+\text{FN}} \quad (37)$$

3. RESULTS AND DISCUSSION

The presented techniques were implemented using MATLAB R2018 on Windows 10 64-bit operating system, Intel®Core™ i5-2540M CPU@2.60GHz central processing unit (CPU), 6 GB random access memory (RAM) and 500 GB hard disk drive. The application was designed to run across different platforms. A total number of 280 mammographic images were used to test the techniques. Three (3) techniques were evaluated; This includes WA-GSA which combines Gabor and GLCM optimum features, Gabor features and GLCM features. The result of the feature extractions was presented and evaluated for each of the techniques. Table 1 presents the contingency table for SVM classification using WA-GSA, Gabor and GLCM features. The mammogram dataset comprises of 280 images out of which 93 were Normal and 187 were abnormal (Benign/Malignant).

Table 1 summarizes the WA-GSA, Gabor and GLCM features as shown, the SVM techniques with WA-GSA features properly classified 84 of the normal mammogram datasets as normal as against the recorded 81 for Gabor and 76 for GLCM. WA-GSA algorithm equally performed better in terms of the corresponding false negatives as recorded. Similarly, the classification of the abnormal dataset performed better by correctly identifying 184 of the abnormal datasets as abnormal as against the 181 and 179 recorded for Gabor and GLCM, respectively. Table 1 shows the superiority of WA-GSA over Gabor and GLCM in terms of the confusion matrix.

Table 1. Contingency table for classification using WA-GSA, Gabor and GLCM features

Techniques		WA-GSA		Gabor		GLCM	
		Predicted Class		Predicted Class		Predicted Class	
Actual Class	Normal (93)	84 (TP)	9 (FN)	81 (TP)	12 (FN)	76 (TP)	17 (FN)
	Abnormal (187)	3 (FP)	184 (TN)	6 (FP)	181 (TN)	8 (FP)	179 (TN)

Weighted average gravitational search algorithm (WA-GSA); Gray level co-occurrence matrices (GLMC)

Furthermore, Table 2 depicts the performance of WA-GSA, Gabor and GLCM feature for validation measures; FPR, FNR, accuracy, and computation time. The result obtained in Table 3 shows that at $\gamma = 3$ and $C=1,000$; the SVM technique achieved FPR, FNR and accuracy of 1.60%, 9.68% and 95.51% at 271.83 seconds, respectively, for WA-GSA features. Also, the SVM technique achieved FPR, FNR and accuracy of 3.21%, 12.90% and 93.57% at 2351.29 seconds, respectively, for Gabor features. Similarly, the SVM technique achieved FPR, FNR and accuracy of 4.28%, 18.28% and 91.07% at 384.54 seconds, respectively, for GLCM features.

Table 2. WA-GSA, Gabor and GLCM features for SVM classification

Technique	FPR (%)	FNR (%)	Accuracy (%)	Time (sec)
WA-GSA	1.60	9.68	95.71	271.83
GABOR	3.21	12.90	93.57	2351.29
GLCM	4.28	18.28	91.07	384.54

Table 2 presents the WA-GSA, Gabor, GLCM features for the SVM classification. As observed, the WA-GSA features outperformed both the Gabor and GLCM features in terms of FPR, FNR, accuracy and computation time. Additionally, validation measures namely FPR, FNR, accuracy and computation time exhibit superiority of WA-GSA features over both Gabor and GLCM features. Figures 4 and 5 depict the relationship between the computation time and gamma value as well as the accuracy and gamma values, respectively.

Table 3 summarizes the statistical comparison between WA-GSA, Gabor and GLCM features. Inferential statistical analysis using paired sampled t-test was done to analyze the result obtained for WA-GSA and Gabor features, and for WA-GSA and GLCM features with accuracy, FPR, FNR and computation time reveal that the test of significance of the aforementioned metrics evaluated at 95% confidence level shows that there was a significant difference between WA-GSA features and Gabor features as well as WA-GSA features and GLCM features at $P<0.05$. The t-test result validates the fact that the SVM technique with WA-GSA features outperformed the SVM technique with both Gabor features and GLCM

features in terms of accuracy, FPR, FNR and computation time in the classification of mass in digital mammography.

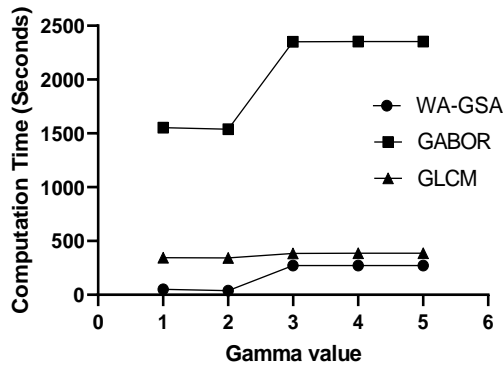


Figure 4. Variation of computation time versus gamma value

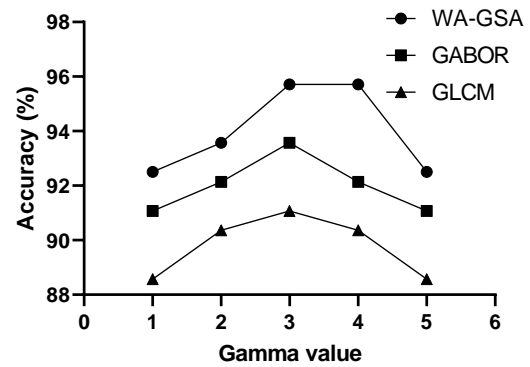


Figure 5 Variation of accuracy versus gamma value

Table 3. Statistical comparison between WA-GSA, Gabor and GLCM feature on paired sampled t-test at 0.05 significance level

Techniques	Measures	Mean difference	t value	p-value
WA-GSA vs GLCM	Accuracy	4.21	11.59	.000
	FPR	-3.00	-7.52	.002
	FNR	-6.66	-6.08	.004
	C-Time	-187.69	-4.13	.014
WA-GSA vs Gabor	Accuracy	2.00	4.81	.009
	FPR	-1.50	-4.79	.009
	FNR	-3.01	-4.81	.009
	C-Time	-1849.11	-13.02	.000

*Computation time (C-Time); False negative rate (FNR); False positive rate (FPR)

The outcome of this study justifies the combination of optimized features of GLCM and Gabor using WA-GSA technique. The combined textural features from WA-GSA technique achieved a more discriminating and computationally efficient feature which reduces both high false positive and negative rates associated with existing techniques in digital mammography. The result achieved in this study signifies that the gamma value is an important parameter of SVM which has a great influence on the accuracy and complexity of the classification models as supported by [26], [27].

The work in this study is in consonant with the work of Suresh *et al.* [28] that used hybrid features involving GLCM to achieve improved performance in the classification of mass. Also, the findings in this study corroborate the works of Fardin and Hassan [29] who combined Gabor and fast GLCM features to achieve a more discriminating feature in the classification of very high-resolution remote sensing images. This is also applicable in this study; the combination of the Gabor and GLCM features also achieved improved discriminating features for the classification of masses in digital mammography. Furthermore, based on the suggestion of Khan *et al.* [18] which stated that the reduction of features in the Gabor filter bank is required to reduce time complexity in the classification of mammograms and the submission of Xing and Jia [17] which stated that GLCM features also tend to have a high computationally complexity; the application of WA-GSA technique was able to achieve a combine optimum features from Gabor and GLCM features with reduced computational complexity. Hence, WA-GSA technique achieved improved discriminating features which are less computationally expensive with reduced false positive and false negative in the classification of masses in digital mammography.

4. CONCLUSION

In this study, the WA-GSA was used to fuse and optimize Gabor and GLCM features in the classification of masses in digital mammography. The results achieved in this study showed that the proposed hybrid feature extraction technique would reduce rate of false positive and false negative diagnosis by 1.61% and 3.22% respectively when compared with Gabor technique and 2.68% and 8.60% respectively when compared with GLCM technique. Additionally, the result showed that the proposed hybrid feature extraction

technique would reduce the computational time by 2079.46 and 112.71 seconds when compared with Gabor and GLCM technique respectively. It was evident that the WA-GSA was well matched to some other existing conventional textural feature extraction method based on its performance. The WA-GSA features will achieve a more accurate and computationally efficient CAD system which will help radiologists' interpretation of mammograms for detection of lesions and classification. The results have demonstrated the efficacy and accuracy of the proposed method of helping the radiologist on diagnosing breast cancer. It is considered a sufficient method to extract features that can assist in avoiding tumor classification difficulties and false-positive reduction. It should be considered in building a truly accurate and computationally efficient CAD system which will help radiologists in accurate interpretation of mammograms for detection of lesions and classification. Also, it could be adopted in clinical practices for better detection and classification of breast cancer.




REFERENCES

- [1] S. Punitha, R. Subban, M. Devi, and J. Vaishnavi, "Breast cancer detection using classification techniques in digital mammography," *International science press. IJCTA*, vol. 9, pp. 3123–3134, 2016.
- [2] M. A. Berbar, "Hybrid methods for feature extraction for breast masses classification," *Egyptian Informatics Journal*, vol. 19, no. 1, pp. 63–73, Mar. 2018, doi: 10.1016/j.ej.2017.08.001.
- [3] M. Y. Kamil, "Computer aided diagnosis for breast cancer based on the Gabor filter technique," *International Journal of Electrical and Computer Engineering (IJECE)*, vol. 10, no. 5, pp. 5235–5243, Oct. 2020, doi: 10.11591/ijece.v10i5.pp5235-5242.
- [4] C. Muramatsu, T. Hara, T. Endo, and H. Fujita, "Breast mass classification on mammograms using radial local ternary patterns," *Computers in Biology and Medicine*, vol. 72, pp. 43–53, May 2016, doi: 10.1016/j.combiomed.2016.03.007.
- [5] A. Sakai *et al.*, "A method for the automated classification of benign and malignant masses on digital breast tomosynthesis images using machine learning and radiomic features," *Radiological Physics and Technology*, vol. 13, no. 1, pp. 27–36, Mar. 2020, doi: 10.1007/s12194-019-00543-5.
- [6] L. C. S. Romualdo, M. A. C. Vieira, H. Schiabel, N. D. A. Mascarenhas, and L. R. Borges, "Mammographic image denoising and enhancement using the anscombe transformation, adaptive wiener filtering, and the modulation transfer function," *Journal of Digital Imaging*, vol. 26, no. 2, pp. 183–197, Apr. 2013, doi: 10.1007/s10278-012-9507-1.
- [7] J. Dheeba, N. Albert Singh, and S. Tamil Selvi, "Computer-aided detection of breast cancer on mammograms: A swarm intelligence optimized wavelet neural network approach," *Journal of Biomedical Informatics*, vol. 49, pp. 45–52, Jun. 2014, doi: 10.1016/j.jbi.2014.01.010.
- [8] M. Talha, "Classification of mammograms for breast cancer detection using fusion of discrete cosine transform and discrete wavelet transform features," *Biomedical Research*, vol. 27, no. 2, 2016.
- [9] E. Rashedi, H. Nezamabadi-pour, and S. Saryazdi, "GSA: A gravitational search algorithm," *Information Sciences*, vol. 179, no. 13, pp. 2232–2248, Jun. 2009, doi: 10.1016/j.ins.2009.03.004.
- [10] F. Shirazi and E. Rashedi, "Feature weighting for cancer tumor detection in mammography images using gravitational search algorithm," in *2016 6th International Conference on Computer and Knowledge Engineering (ICCKE)*, Oct. 2016, pp. 310–313, doi: 10.1109/ICCKE.2016.7802158.
- [11] S. Khan, A. Khan, M. Maqsood, F. Aadil, and M. A. Ghazanfar, "Optimized Gabor feature extraction for mass classification using cuckoo search for big data e-healthcare," *Journal of Grid Computing*, vol. 17, no. 2, pp. 239–254, Jun. 2019, doi: 10.1007/s10723-018-9459-x.
- [12] Y. Kang *et al.*, "Texture analysis of torn rotator cuff on preoperative magnetic resonance arthrography as a predictor of postoperative tendon status," *Korean Journal of Radiology*, vol. 18, no. 4, p. 691, 2017, doi: 10.3348/kjr.2017.18.4.691.
- [13] M. Maktabdar Oghaz, M. A. Maarof, M. F. Rohani, A. Zainal, and S. Z. M. Shaid, "An optimized skin texture model using gray-level co-occurrence matrix," *Neural Computing and Applications*, vol. 31, no. 6, pp. 1835–1853, Jun. 2019, doi: 10.1007/s00521-017-3164-8.
- [14] F. I. Alam and R. U. Faruqi, "Optimized calculations of haralick texture features," *European Journal of Scientific Research*, vol. 50, pp. 543–553, 2011.
- [15] L.-K. Soh and C. Tsatsoulis, "Texture analysis of SAR sea ice imagery using gray level co-occurrence matrices," *IEEE Transactions on Geoscience and Remote Sensing*, vol. 37, no. 2, pp. 780–795, Mar. 1999, doi: 10.1109/36.752194.
- [16] H. Liu, T. Tan, J. van Zelst, R. Mann, N. Karssemeijer, and B. Platel, "Incorporating texture features in a computer-aided breast lesion diagnosis system for automated three-dimensional breast ultrasound," *Journal of Medical Imaging*, vol. 1, no. 2, 24501, Jul. 2014, doi: 10.1117/1.jmi.1.2.024501.
- [17] Z. Xing and H. Jia, "An improved thermal exchange optimization based GLCM for multi-level image segmentation," *Multimedia Tools and Applications*, vol. 79, no. 17–18, pp. 12007–12040, May 2020, doi: 10.1007/s11042-019-08566-1.
- [18] S. Khan, M. Hussain, H. Aboalsamh, H. Mathkour, G. Bebis, and M. Zakariah, "Optimized Gabor features for mass classification in mammography," *Applied Soft Computing*, vol. 44, pp. 267–280, Jul. 2016, doi: 10.1016/j.asoc.2016.04.012.
- [19] M. Hussain, S. Khan, G. Muhammad, I. Ahmad, and G. Bebis, "Effective extraction of Gabor features for false positive reduction and mass classification in mammography," *Appl. Math. Inf. Sci.*, vol. 6, no. 1, pp. 29–33, 2012.
- [20] A. A. Khan, M. Khan, and A. S. Arora, "Automatic detection of malignant neoplasm from mammograms," in *2015 Science and Information Conference (SAI)*, Jul. 2015, pp. 292–297, doi: 10.1109/SAI.2015.7237158.
- [21] J. C. Bezdek, R. Ehrlich, and W. Full, "FCM: The fuzzy c-means clustering algorithm," *Computers and Geosciences*, vol. 10, no. 2–3, pp. 191–203, Jan. 1984, doi: 10.1016/0098-3004(84)90020-7.
- [22] M. V. Madhavi and T. C. Bobby, "Gabor filter based classification of mammography images using LS-SVM and random forest classifier," in *Communications in Computer and Information Science*, Springer Singapore, 2019, pp. 69–83.
- [23] Z. Sun, G. Bebis, and R. Miller, "Monocular precrash vehicle detection: features and classifiers," *IEEE Transactions on Image Processing*, vol. 15, no. 7, pp. 2019–2034, Jul. 2006, doi: 10.1109/TIP.2006.877062.
- [24] V. N. Vapnik, *The nature of statistical learning theory*. New York, NY: Springer New York, 2000.
- [25] C. J. C. Burges, "A tutorial on support vector machines for pattern recognition," *Data Mining and Knowledge Discovery*, vol. 2, no. 2, pp. 121–167, 1998.




- [26] C. Savas and F. Dervis, "The impact of different kernel functions on the performance of scintillation detection based on support vector machines," *Sensors*, vol. 19, no. 23, Nov. 2019, doi: 10.3390/s19235219.
- [27] A. Tharwat and T. Gabel, "Parameters optimization of support vector machines for imbalanced data using social ski driver algorithm," *Neural Computing and Applications*, vol. 32, no. 11, pp. 6925–6938, Jun. 2020, doi: 10.1007/s00521-019-04159-z.
- [28] R. Suresh, A. N. Rao, and B. E. Reddy, "Detection and classification of normal and abnormal patterns in mammograms using deep neural network," *Concurrency and Computation: Practice and Experience*, vol. 31, no. 14, Jul. 2019, doi: 10.1002/cpe.5293.
- [29] M. Fardin and G. Hassan, "Fast GLCM and Gabor filters for texture classification of very high resolution remote sensing images," *International Journal of Information, and Communication Technology Research*, vol. 7, no. 3, pp. 21–30, 2015.

BIOGRAPHIES OF AUTHORS






Oludare Yinka Ogundepo    received the B.Tech. degree from the Department of Electrical and Electronics Engineering, Faculty of Engineering, Ladoko Akintola University of Technology, Ogbomoso, Nigeria, in 2009, the M.ENG. degree from the Federal University of Technology Akure, Nigeria, in 2015. He is currently on his Ph.D. degree in Electrical and Electronics engineering from the University of Ilorin, Nigeria. His current research interests include RF theory, signal processing, image processing, artificial intelligence, and computer vision. He can be contacted at email: oludare.ogundepo@fupre.edu.ng.



Isaac Ozovehe Avazi Omeiza    received the B.Eng. and M.Eng. degrees in Electrical Engineering from University of Ilorin, Nigeria, in 1990 and 2000 respectively. He further obtained a Ph.D. in Electrical Engineering from the same university in 2007. His major research interests include: image analysis, pattern recognition, computer vision, and digital systems. He is presently a member of faculty in the Department of Electrical and Electronics Engineering at University of Ilorin, Kwara State, Nigeria. He can be contacted at email: isaacavazi@unilorin.edu.ng.



Jonathan Ponnmile Oguntoye    received the B.Tech. and M.Tech. degree from the Department of Computer Science and Engineering, Faculty of Engineering and Technology, Ladoko Akintola University of Technology (LAUTECH), Ogbomoso, Nigeria, in 2010 and 2018 respectively. He is currently on his Ph.D. degree in computer engineering in Lautech, Nigeria. His current research interests include image processing, biometrics, soft computing, and information systems. He can be contacted at email: jponguntoye@lautech.edu.ng.